




Complex fragment emission in dissipative binary decay of $^{74,76}\text{Kr}$

T. K. Rana ^{1,2,*}, Samir Kundu^{1,2}, C. Bhattacharya^{1,2}, S. Manna^{1,2}, Pratap Roy ^{1,2}, R. Pandey¹, A. Sen^{1,2}, T. K. Ghosh^{1,2}, G. Mukherjee ^{1,2}, K. Banerjee^{1,2}, S. Mukhopadhyaya^{1,2}, D. Paul^{1,2}, Md. Moin Shaikh^{1,†}, S. Nandi^{1,2}, Vishal Srivastava³, J. K. Sahoo¹, J. K. Meena¹, A. K. Saha¹, R. M. Saha¹, Somnath Dalal¹ and S. Bhattacharya^{1,‡}

¹Variable Energy Cyclotron Centre, I/AF, Bidhan Nagar, Kolkata-700064, India

²Homi Bhabha National Institute, Training School Complex, Anushakti Nagar, Mumbai-400094, India

³Racah Institute of Physics, The Hebrew University of Jerusalem, Jerusalem 91904, Israel



(Received 9 November 2020; revised 15 January 2021; accepted 11 February 2021; published 19 March 2021)

The fragment emission mechanism in the binary decay of composites formed in the reactions $^{20}\text{Ne}+^{56}\text{Fe}$ and $^{16}\text{O}+^{58}\text{Ni}$ has been studied at two different excitation energies. The inclusive energy and angular distributions of the emitted fragments $^6,7\text{Li}$, $^7,8,9\text{Be}$, $^{10,11}\text{B}$, and $^{11,12,13,14}\text{C}$ have been measured in the laboratory angles ranging from 15° to 35° (corresponding angles in center of mass ranging from 20° to 50°). The energy distributions of the fragments are found to be Gaussian and peaked at energies higher than those expected from fusion-fission-type reactions. The center-of-mass angular distributions of all the fragments have been found to fall faster than $\approx 1/\sin\theta_{\text{c.m.}}$ -like dependence and the average Q values of the fragments are found to decrease with increasing the center-of-mass angle of the emitted fragment for both the systems. The above characteristics of fragments signify that they were emitted from nonequilibrium sources, produced in a highly energy damped deep-inelastic-type reaction. The lifetimes of the dinuclear composites estimated from the angular distributions of these fragments are found to be in the range of $\approx(0.5-2.7)\times 10^{-22}$ s, which are smaller than the respective compound-nuclear lifetimes [$\approx(1.0-2.0)\times 10^{-21}$ s]. The angular-momentum dissipations estimated from the average kinetic energies of the fragments are found to be, for lighter fragments in particular, greater than those predicted by the empirical sticking limit.

DOI: [10.1103/PhysRevC.103.034614](https://doi.org/10.1103/PhysRevC.103.034614)

I. INTRODUCTION

The study of complex fragment emission is a standard technique to explore the dynamics of breakup of hot composite formed in heavy-ion collisions [1–20]. It has been studied theoretically [1–4] as well as experimentally [5–20] quite extensively; however, there are several unanswered questions remaining to be explored. In recent times, with the advent of more sophisticated and advanced experimental tools more and more in-depth understanding of the entrance channel dynamics of the reaction could be achieved. The gross mechanism behind complex fragment emission is now quite well understood at low excitation; however, there remains some gaps in the understanding at high excitation energy, particularly well above the Coulomb barrier [21]. Several known mechanisms contribute to the phenomenon, e.g., complete equilibrium processes like fusion evaporation (FE) or fusion-fission (FF) and/or nonequilibrium processes like quasi-elastic (QE) [22,23], deep-inelastic (DI), incomplete fusion, and deep-inelastic orbiting processes [6–11]. Whereas the FF process dominates at lower beam energies, deep-inelastic re-

actions become increasingly dominant at higher energies (well above the Coulomb barrier).

The study of deep-inelastic reactions is of current interest both experimentally and theoretically because they can be used as a probe to look into several complex dynamical features of nuclear interaction like the mechanism of nucleon transport and nuclear dissipation. These reactions, being intermediate between direct- and compound-nuclear reactions, exhibit characteristics of both direct- as well as compound-nuclear reactions. As the beam energy, the orbital angular momentum, the charge product of target and projectile, or the mass asymmetry of the collision partner increases, the DI cross section increases with a corresponding decrease in FF probability [24]. Significant mass flow may occur during the interaction time of such collisions. This type of reaction is characterized by nonequilibrated exit channel mass distributions (retaining strong memory of entrance channel), and, at the same time complete or large damping of the energy and angular momentum of relative motion [25,26].

The relaxation of various degrees of freedom (N/Z , E) in deep-inelastic collisions may be uniquely studied through the isotopic mass and energy distributions of the emitted fragments [27–29]. However, most such studies have so far been done for heavier systems [projectile mass (A_p) + target mass (A_t) > 100], and experimental measurements on the DI fragment emission for $A_p + A_t < 100$ are scarce. In the present article, the complex fragment emission mechanism has been

*tapan@vecc.gov.in

[†]Present address: Department of Physics, Chanchal College, Chanchal, Malda, West Bengal-732123, India.

[‡]Retired.

studied in the two reactions $^{20}\text{Ne} + ^{56}\text{Fe}$ and $^{16}\text{O} + ^{58}\text{Ni}$ at high excitation energy well above the Coulomb barrier. Here, we report a comparative study of the reactions with different (N/Z) ratio in the entrance channel at $\approx 7\text{--}10$ MeV/nucleon beam energies.

The article has been arranged as follows: Experimental details have been described in Sec. II, data analysis has been discussed in Sec. III. Results and discussions have been presented in Sec. IV. Finally, the conclusions have been given in Sec. V.

II. EXPERIMENTAL DETAILS

The experiment was performed at the Variable Energy Cyclotron Centre, Kolkata, India using ^{20}Ne (147.5 and 166.5 MeV) and ^{16}O (143.8 and 161.6 MeV) beams on ^{56}Fe (natural) and ^{58}Ni (purity: $\approx 99.5\%$) targets, respectively. The beam energies have been chosen to populate the composites at the same excitation energies. The emitted fragments have been detected in the laboratory (lab) angle from 15° to 35° using two silicon strip detector telescopes of the ChAKRA array [30]. Each telescope consisted of (i) $\approx 50\ \mu\text{m}$, single-sided silicon strip (16 channels) ΔE detector and (ii) $\approx 1030\ \mu\text{m}$, double-sided silicon strip (16×16 channels) E detector [30]. The angular resolution of each strip in both the telescopes was $\approx 1^\circ$. Energy calibrations of the telescopes were performed using a ^{229}Th - α source and the elastic peaks obtained from the scattering of beams on ^{197}Au target at different energies. A VERSA Module Eurocard (VME)-based online data-acquisition system was used for acquiring online data [31,32]. The systematic errors in the data, arising from the uncertainties in the measurements of the solid angle, target thickness, and the calibration of current digitizer have been estimated to be $\approx 10\%$. The total uncertainty has been considered as the quadratic sum of systematic and the statistical uncertainties. Typical two-dimensional particle identification plots obtained for a single strip of ΔE vs E are shown in Figs. 1(a) and 1(b) for the reactions $^{20}\text{Ne} + ^{56}\text{Fe}$ (166.5 MeV) and $^{16}\text{O} + ^{58}\text{Ni}$ (161.6 MeV), respectively. From Fig. 1, it has been observed that isotopic separation obtained for different fragments in both the reactions was quite satisfactory.

III. DATA ANALYSIS

A. Energy distributions

Typical inclusive double-differential energy spectra (black solid line), $d^2\sigma/d\Omega dE$, in the laboratory, for different isotopes of the fragments (Li-C) obtained in the decay of the composites have been shown in Figs. 2 and 3 for the reactions $^{20}\text{Ne} + ^{56}\text{Fe}$ and $^{16}\text{O} + ^{58}\text{Ni}$, respectively. The energy of each isotope was corrected for energy losses in the target thickness as well as for energy losses in detector dead layers. The energy distributions are found to be nearly Gaussian in shape (excluding the transfer channel peaks), having their centroid at the an energy higher than the expected kinetic energies for the fission fragments obtained from the Viola systematics corrected by the corresponding asymmetry factors [33,34] (shown by blue arrows in Figs. 2 and 3).

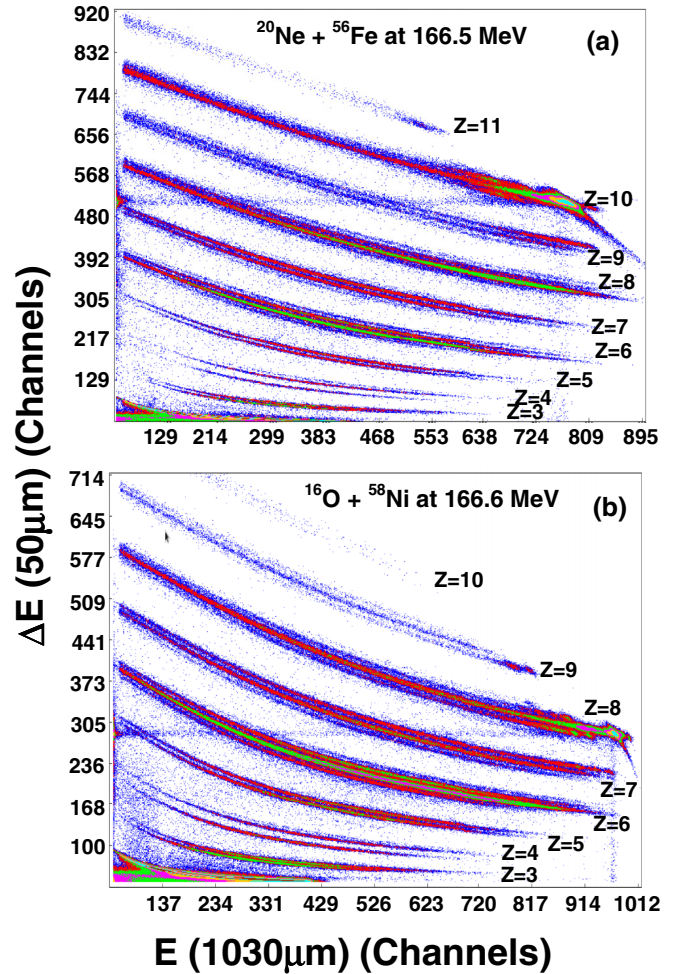


FIG. 1. Two-dimensional particle identification spectra (a) for the reaction $^{20}\text{Ne} + ^{56}\text{Fe}$ at 166.5 MeV and (b) for the reaction $^{16}\text{O} + ^{58}\text{Ni}$ at 161.6 MeV at an angle $\approx 20^\circ$ in the laboratory.

The energy spectra of ^8Be were reconstructed from the measured 2α coincidence events in both the reactions. The ^8Be ground-state decay events are expected to form a peak around the relative energy of ≈ 92 keV, i.e., the breakup threshold of ^8Be into 2α . Therefore, the corresponding ^8Be energy spectra have been generated by gating the relative energy of ≈ 92 keV between all detected 2α events. The corresponding energy spectra of ^8Be at 20° in the laboratory are shown in Figs. 4(a), 4(b) and 4(c), 4(d) for the reactions $^{20}\text{Ne} + ^{56}\text{Fe}$ and $^{16}\text{O} + ^{58}\text{Ni}$ at two different beam energies, respectively. The energy spectra have been corrected for efficiency of the experimental setup, which has been estimated by using a Monte Carlo simulation [35–37]. It is observed from the above figures that the energy spectrum of ^8Be is also peaked at an energy higher than that obtained from the Viola systematics corrected by the corresponding asymmetry factors [33,34] (shown by blue arrows in Fig. 4) for both systems.

The FF components of the reaction are expected to be peaked around the Viola energy (blue arrow shown in Figs. 2 to 4). From the above figures, it has been observed that the Viola peak for all the isotopes are near the leading edge of the

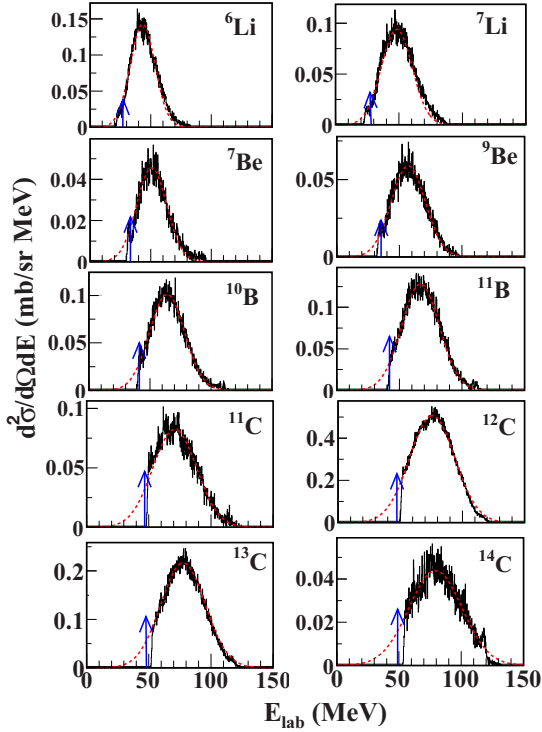


FIG. 2. Energy distributions of different isotopes of the fragments (Li-C) (black solid lines) for the reaction ^{20}Ne (166.5 MeV) + ^{56}Fe at an angle $\approx 20^\circ$ in the laboratory. Arrows (in blue color) indicate the mean kinetic energies of the fragments obtained from Viola systematics corrected by the corresponding asymmetry factors, and red dotted lines are the fitted Gaussian used to extract the yields of the fragments.

energy spectrum. Therefore, even if there is any contribution from FF processes, it only remains in the tail part of the energy distributions. Hence, in the present analysis, the contribution of FF processes has been neglected and assumed to be only the nonfusion type of contribution. The nonfusion contribution at each angle has been estimated by fitting the respective measured energy spectrum with a Gaussian function (shown by red dotted lines in Figs. 2 to 4).

B. Angular distributions

The center of mass (c.m.) angular distribution ($d\sigma/d\Omega$) of the fragment cross section carries the signature of the reaction emission mechanism. For example, FF or compound-nucleus-type reactions are characterized by an angular distribution that is symmetric around 90° in the c.m. and, in the classical limit, is of the form $d\sigma/d\Omega \approx 1/\sin\theta_{\text{c.m.}}$. On the other hand, for the highly damped DI-type process, the angular distributions will be forward peaked. The extracted fragment angular distributions in the c.m. frame for different isotopes of the fragments (Li-C) are shown in Figs. 5 and 6 for the reaction $^{20}\text{Ne} + ^{56}\text{Fe}$ (composite ^{76}Kr) at two different beam energies, respectively. For the system $^{16}\text{O} + ^{58}\text{Ni}$ (composite ^{74}Kr), the extracted angular distributions at two different beam energies are shown in Figs. 7 and 8, respectively. The angular distributions of all fragments emitted in both the

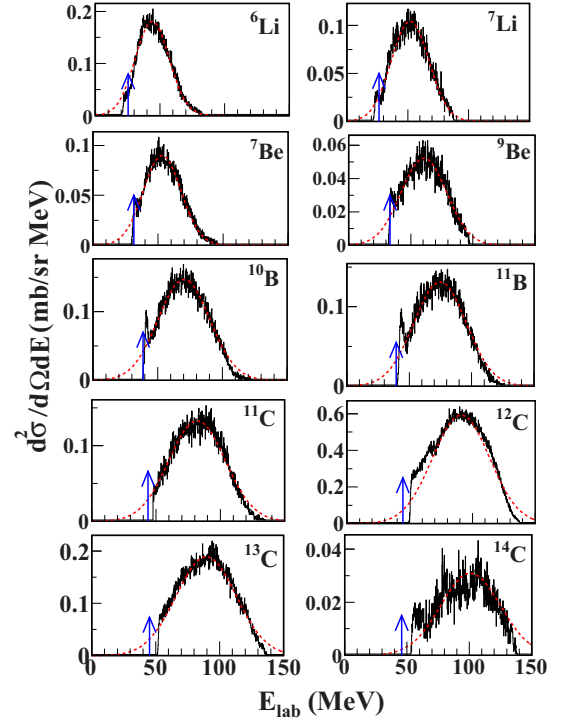


FIG. 3. Same as Fig. 2 but for the reaction $^{16}\text{O} + ^{58}\text{Ni}$ at 161.6 MeV.

reactions (at both beam or excitation energies) are found to fall faster than $\approx 1/\sin\theta_{\text{c.m.}}$, which demonstrates that these fragments are emitted from a process faster than the CN or FF process.

C. Time period of rotations

The time period of rotation of the target and projectile or the lifetime of the intermediate dinuclear complex can be estimated from the angular distributions (Figs. 5–8) of the fragments using a diffractive Regge-pole model [38,39]. The angular distribution of each fragment has been fit with the

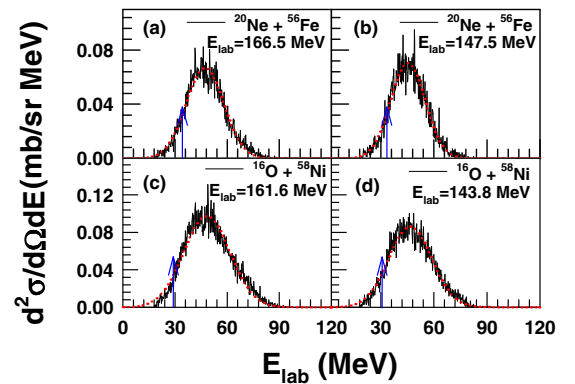


FIG. 4. Energy distributions of ^8Be reconstructed from the 2α coincidence events in reaction (a), (b) $^{20}\text{Ne} + ^{56}\text{Fe}$ and (c), (d) $^{16}\text{O} + ^{58}\text{Ni}$ at an angle $\approx 20^\circ$ in laboratory.

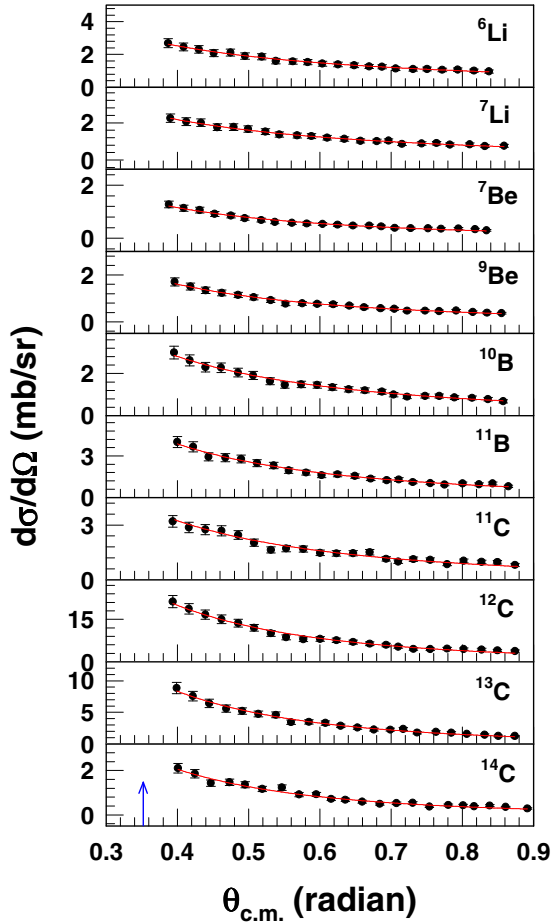


FIG. 5. The center of mass (c.m.) angular distributions of different isotopes of the fragments (Li-C) for the reaction $^{20}\text{Ne} + ^{56}\text{Fe}$ at 166.5 MeV. The solid circles are the experimental data and red lines correspond to the fit to the data obtained using Eq. (1). Arrows (in blue) indicate the grazing angle for the reaction.

following expression:

$$\frac{d\sigma}{d\Omega} = \frac{a}{\sin(\theta_{\text{c.m.}})} e^{-\theta_{\text{c.m.}}/\theta_0}, \quad (1)$$

where a is the constant of proportionality and θ_0 is the “life angle” of the composite after the reaction. Equation (1) describes the decay of a rotating dinucleus with an angular velocity $\omega = \hbar/\mu R^2$, where μ represents the reduced mass of the system, l is the angular momentum ($l_{\text{cr}} \leq l \leq l_{\text{gr}}$; l_{cr} , l_{gr} being the critical angular momentum for fusion and the grazing angular momentum, respectively), and R represents the distance between the two centers of the dinucleus. The “life angle” θ_0 is then the product of angular velocity ω and the rotation time τ , where τ is the time interval during which the two nuclei remain in contact in the form of the rotating dinuclear composite. The characteristics of a reaction process depend on the value of θ_0 . Smaller values of θ_0 are associated with faster processes for which the corresponding angular distributions are more forward peaked. Large values of θ_0 ($\geq 2\pi$) are associated with slow processes with lifetimes that are large or comparable to the dinucleus

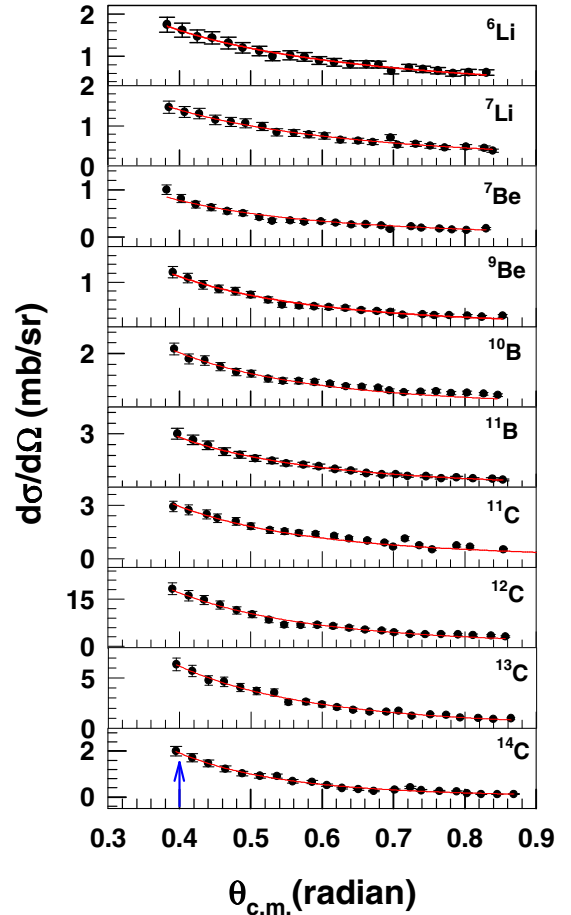


FIG. 6. Same as Fig. 5 but for the reaction $^{20}\text{Ne} + ^{56}\text{Fe}$ at 147.5 MeV.

rotation period $\tau_{\text{rot}} (=2\pi/\omega)$, in the present case are found to be $\approx(1.2-1.5) \times 10^{-21}\text{s}$, $\approx(1.3-1.6) \times 10^{-21}\text{s}$, $\approx(1.0-1.3) \times 10^{-21}\text{s}$, and $\approx(1.1-1.4) \times 10^{-21}\text{s}$ for 166.5 and 147.5 MeV in $^{20}\text{Ne} + ^{56}\text{Fe}$ and 161.6 and 143.8 MeV in $^{16}\text{O} + ^{58}\text{Ni}$ systems, respectively. For lifetimes $\geq \tau_{\text{rot}}$, long-lived configurations are assumed to be formed, and the angular distributions tend to become symmetric around 90° in the c.m. frame ($d\sigma/d\Omega \approx 1/\sin\theta_{\text{c.m.}}$ -type distribution). The FF process is thus a limiting case of the DI process, where a very long-lived configuration is assumed to be formed and the angular distribution becomes $\approx 1/\sin\theta_{\text{c.m.}}$. The timescales obtained using Eq. (1) are given in Tables I and II for different fragments emitted in the reactions $^{20}\text{Ne} + ^{56}\text{Fe}$ and $^{16}\text{O} + ^{58}\text{Ni}$, respectively. The upper (lower) limit of τ corresponds to the estimate with $l = l_{\text{cr}}$ (l_{gr}). It is clear from Tables I and II that the fragment emission lifetimes are significantly smaller than the corresponding rotational time periods ($\tau \ll \tau_{\text{rot}}$)—indicating their nonequilibrium origin. Furthermore, it has been observed that the timescale decreases as the fragment charge increases. This is expected because the emission of heavier fragments (near the projectile) requires fewer nucleon transfers and therefore less time. On the other hand, the emission of lighter fragments requires more nucleon exchanges and therefore longer time.

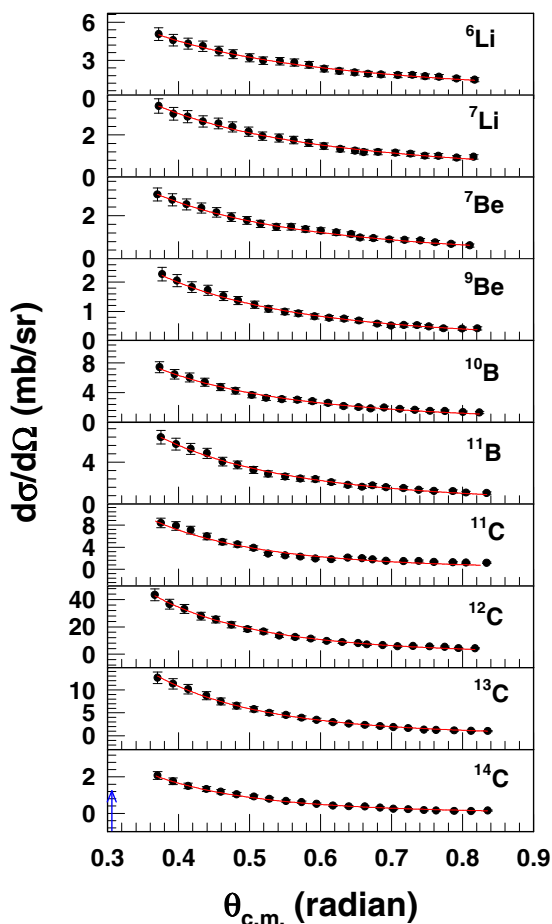


FIG. 7. Same as Fig. 5 but for the reaction $^{16}\text{O} + ^{58}\text{Ni}$ at 161.6 MeV.

D. Q -value distributions

The average Q -value was estimated assuming two-body kinematics and have been displayed as a function of center-of-mass emission angles of the fragments in Figs. 9–12. It is observed that for all isotopes, the Q -value decreases with the increase in center-of-mass emission angle, which is particularly more prominent for the heavy fragments. The slope decreases with decreasing atomic number of the fragment; it implies that the tendency to rotate towards larger negative angles increases with decreasing charge product and/or with increasing angular velocity of the composite nucleus. The figures clearly depict the increased damping of the initial kinetic energy with increasing transfer of charge or increasing angle of emission. At large angles the most probable kinetic energies become nearly constant, indicating that the kinetic-energy damping is complete and dynamic equilibrium has been established before the scission of dinuclear composite takes place.

E. Total cross sections

The total angle-integrated cross sections for all the isotopes have been extracted in both the reactions [shown in Figs. 13(a) and 14(a)] and the corresponding relative cross sections (ratio

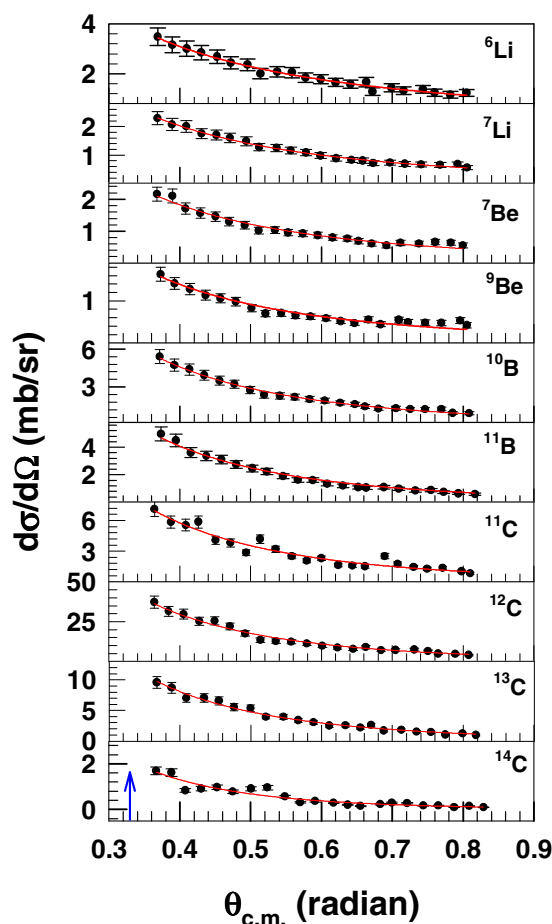


FIG. 8. Same as Fig. 5 but for the reaction $^{16}\text{O} + ^{58}\text{Ni}$ at 143.8 MeV.

of isotopic yields of the reactions $^{20}\text{Ne} + ^{56}\text{Fe}$ and $^{16}\text{O} + ^{58}\text{Ni}$) at two different beam energies are shown in Figs. 13(b) and 14(b), respectively. The yields of the isotopes are found to be more in the breakup of the dinuclear complex ^{74}Kr ($N/Z \approx 1.06$) compared with ^{76}Kr ($N/Z \approx 1.11$) at both the excitation energies. One of the reasons for this is that the breakup thresholds for different isotopes are more for ^{76}Kr compared with ^{74}Kr composite. Alternatively, it can be explained qualitatively due to fewer nucleon exchange required for the ^{16}O projectile compared with the ^{20}Ne projectile to produce the detected isotopes. However, it is observed from Figs. 13(b) and 14(b) that the ratio of isotopic yields of the two reactions increases sharply with the increase of neutron number for all fragments. This observation of preferential emission of more neutron-rich isotopes from comparatively neutron-richer dinuclear composite (^{76}Kr) indicates that the isospin (N/Z) is equilibrated prior to the breakup of the dinuclear composite at these excitation energies. More details have been discussed in the results and discussion section below.

F. Angular-momentum dissipations

One of the interesting features of the DI process is that, apart from dissipation of kinetic energy, there is large

TABLE I. Timescales for emission of various DI fragments for the $^{20}\text{Ne} + ^{56}\text{Fe}$ reaction at two different beam energies. Upper and lower limit corresponds to l_{cr} and l_{gr} , respectively.

E_{lab} (MeV)	l_{cr} (\hbar)	l_{gr} (\hbar)	Fragments (symbol)	Life angle θ_0 (radians)	Lifetime τ (10^{-22} s)			
166.5	59.1	75	^6Li	0.91	2.21(7)–1.74(5)			
			^7Li	0.78	1.89(5)–1.49(4)			
			^7Be	0.48	1.16(3)–0.91(2)			
			^9Be	0.47	1.13(2)–0.89(1)			
			^{10}B	0.42	1.02(2)–0.80(1)			
			^{11}B	0.41	0.98(2)–0.77(2)			
			^{11}C	0.37	0.88(3)–0.70(3)			
			^{12}C	0.34	0.83(1)–0.65(1)			
			^{13}C	0.34	0.82(2)–0.65(1)			
			^{14}C	0.19	0.46(1)–0.36(1)			
			147.5	55.2	68.5	^6Li	1.03	2.66(18)–2.14(14)
						^7Li	0.79	2.05(5)–1.65(4)
						^7Be	0.43	1.12(10)–0.90(8)
						^9Be	0.38	0.99(16)–0.80(12)
^{10}B	0.37	0.96(3)–0.77(2)						
^{11}B	0.36	0.94(2)–0.76(2)						
^{11}C	0.36	0.93(18)–0.75(14)						
^{12}C	0.36	0.93(3)–0.75(2)						
^{13}C	0.34	0.89(7)–0.72(5)						
^{14}C	0.23	0.58(7)–0.47(5)						

dissipation of relative angular momentum into intrinsic angular momentum of the fragments. The emitted fragments from the reaction carry the signatures of nuclear dissipation. Therefore, the measurement of the total kinetic energy of

TABLE II. Same as Table I but for the $^{16}\text{O} + ^{58}\text{Ni}$ reaction at two different beam energies.

E_{lab} (MeV)	l_{cr} (\hbar)	l_{gr} (\hbar)	Fragments (symbol)	life angle θ_0 (radian)	lifetime τ (10^{-22})(s)			
161.6	54.7	71.2	^6Li	0.81	1.71(8)–1.31(7)			
			^7Li	0.64	1.37(12)–1.05(10)			
			^7Be	0.51	1.08(5)–0.83(4)			
			^9Be	0.40	0.85(4)–0.65(3)			
			^{10}B	0.39	0.83(7)–0.63(6)			
			^{11}B	0.37	0.78(5)–0.60(4)			
			^{11}C	0.26	0.55(24)–0.42(19)			
			^{12}C	0.25	0.53(4)–0.41(3)			
			^{13}C	0.25	0.54(4)–0.41(4)			
			^{14}C	0.23	0.50(4)–0.38(3)			
			143.8	51.3	65.65	^6Li	1.05	2.38(18)–1.86(15)
						^7Li	0.60	1.36(13)–1.06(10)
						^7Be	0.51	1.16(5)–0.91(4)
						^9Be	0.44	1.01(5)–0.79(4)
^{10}B	0.39	0.89(8)–0.70(6)						
^{11}B	0.36	0.82(2)–0.64(2)						
^{11}C	0.35	0.81(5)–0.63(4)						
^{12}C	0.32	0.73(5)–0.57(4)						
^{13}C	0.31	0.71(3)–0.55(3)						
^{14}C	0.23	0.52(2)–0.41(2)						

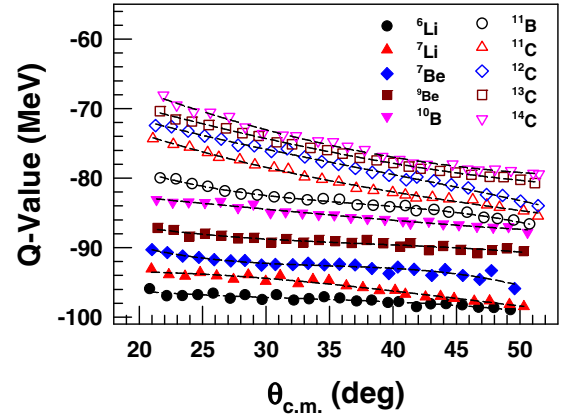


FIG. 9. The Q -value distributions of different isotopes of the fragments (Li-C) for the reaction $^{20}\text{Ne} + ^{56}\text{Fe}$ at $E_{\text{lab}} = 166.5$ MeV. The solid symbols are the experimental data (as marked in figure inset different symbol for different isotopes) and black dashed lines are plotted to guide the eye.

the reaction products offers a direct measure of energy dissipation. Phenomenologically, the kinetic-energy dissipation is due to the friction (radial and tangential) between the surfaces of the rotating dinuclear system; on the other hand, angular-momentum dissipation originates solely from the tangential component of the friction, the magnitude of which is expected to lie between the two limits (rolling and sticking). Estimation of angular momentum in the exit channel depends on another poorly known factor, the scission configuration of the rotating dinuclear system. It is estimated from the total kinetic energy of the rotating dinuclear system. In general, the total kinetic energy E_k of the system at the scission configuration can be estimated by assuming the system as a nuclear molecule in rigid rotation and it may be represented as [20]

$$E_k = V_N(d) + f^2 \frac{\hbar^2 l_i(l_i + 1)}{2\mu d^2}, \quad (2)$$

where $V_N(d)$ is the contribution from Coulomb and nuclear forces at dinuclear separation distance d , μ is the reduced

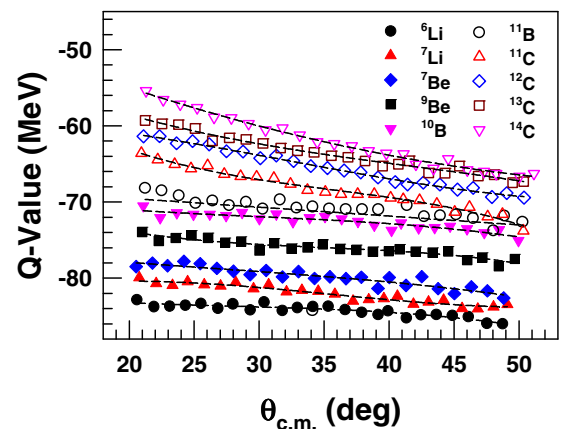


FIG. 10. Same as Fig. 9 but for the reaction $^{20}\text{Ne} + ^{56}\text{Fe}$ at $E_{\text{lab}} = 147.5$ MeV.

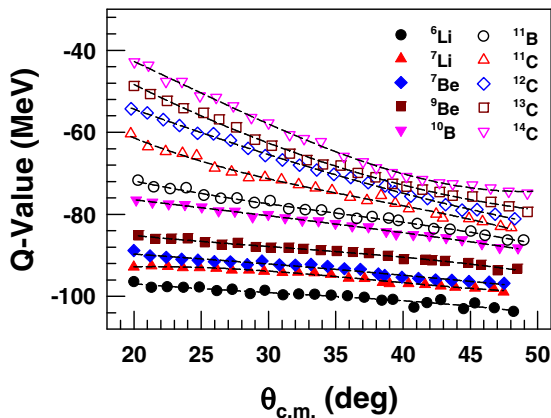


FIG. 11. Same as Fig. 9 but for the reaction $^{16}\text{O} + ^{58}\text{Ni}$ at $E_{\text{lab}} = 161.6$ MeV.

mass of the dinuclear configuration, l_i is the relative angular momentum in the entrance channel, and f is the numerical factor denoting the fraction of the angular-momentum transferred depending on the type of frictional force. A simple procedure for estimating both d and f was given in Ref. [20]. Deep-inelastic collisions are assumed to occur within the angular-momentum window $l_{cr} \leq l \leq l_{gr}$; the fully energy equilibrated dissipative components (at larger angles) correspond to more compact collisions near $l \approx l_{cr}$. However, the fusion-fission yield is also most predominant in the vicinity of $l \approx l_{cr}$. Therefore, the exit channel configurations of both processes are likely to be similar, and it is reasonable to assume a compact scission shape for the fully energy damped DI yield. In the present work, we estimated the separation distance d between the two fragments at the scission point from the Viola peak and its estimated values are 10.6 and 10.7 fm for the reactions $^{20}\text{Ne} + ^{56}\text{Fe}$ and $^{16}\text{O} + ^{58}\text{Ni}$, respectively. Assuming these scission configurations, Eq. (2) has been used to extract the angular-momentum dissipation factor f in DI collisions.

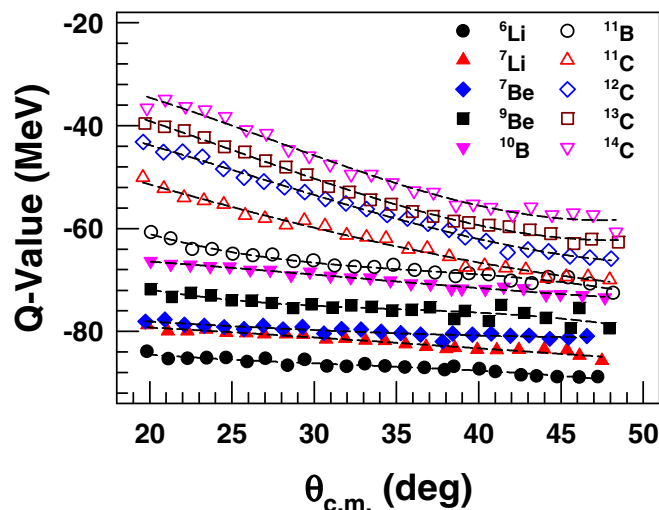


FIG. 12. Same as Fig. 9 but for the reaction $^{16}\text{O} + ^{58}\text{Ni}$ at $E_{\text{lab}} = 143.8$ MeV.

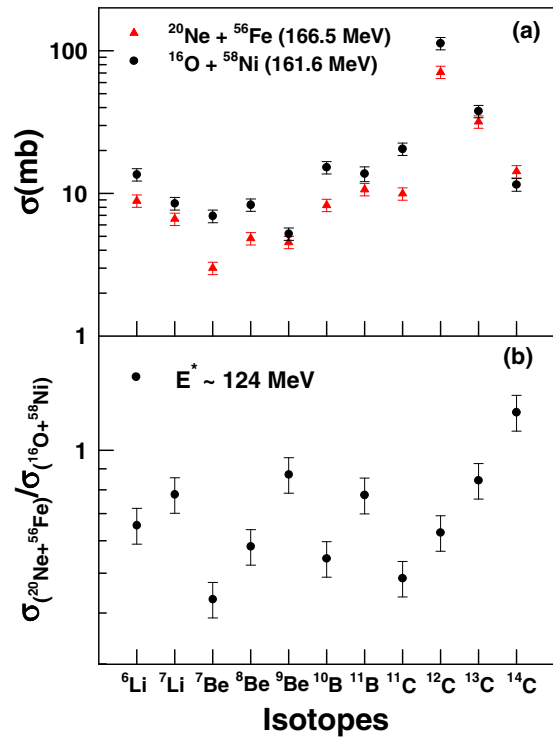


FIG. 13. (a) Total cross sections and (b) ratio of isotopic cross sections obtained for reaction $^{20}\text{Ne} + ^{56}\text{Fe}$ with respect to $^{16}\text{O} + ^{58}\text{Ni}$ reaction at excitation energy ≈ 124 MeV.

The values of f extracted for different energies for these reactions are displayed in Fig. 15 along with the respective rolling (red solid lines) and sticking (black dash lines) limit

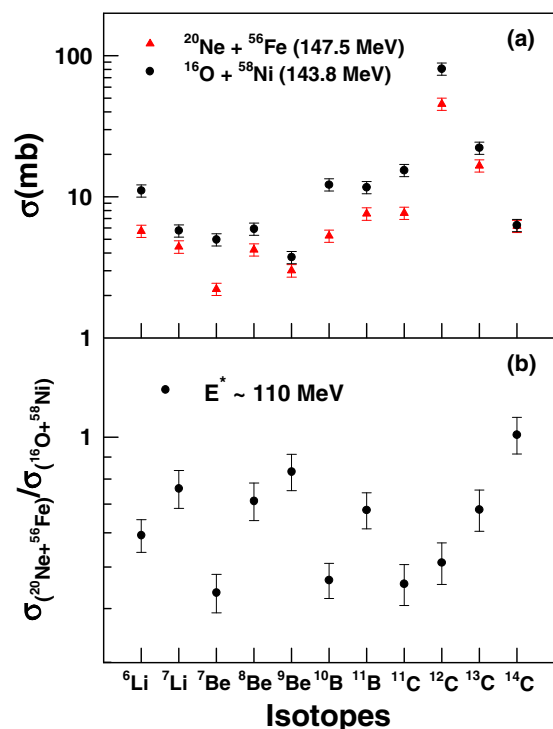


FIG. 14. Same as Fig. 13 but at ≈ 110 MeV excitation energy.

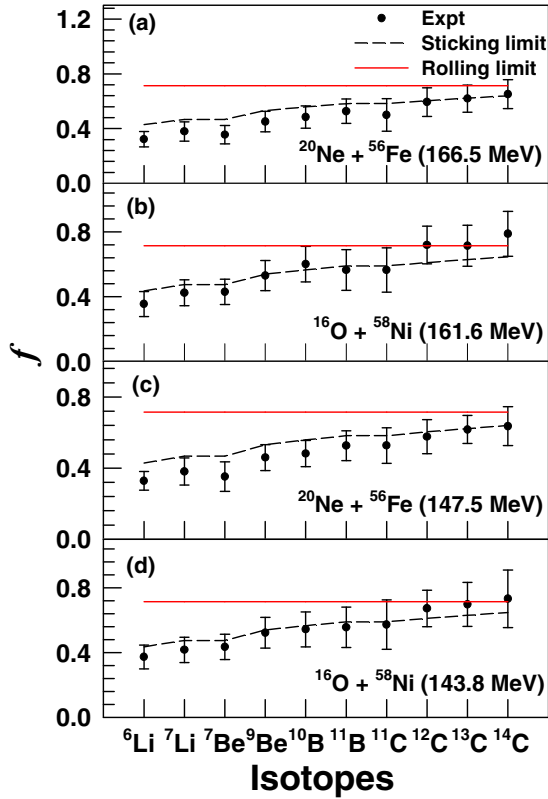


FIG. 15. Variation of angular-momentum dissipation factor f with different isotopes of the fragments (Li-C) in (a), (c) $^{20}\text{Ne} + ^{56}\text{Fe}$ and (b), (d) $^{16}\text{O} + ^{58}\text{Ni}$ reactions. Solid circles are the experimental data. Red solid and black dash lines are the calculation due to rolling and sticking limits, respectively.

predictions. During the calculation the value of initial angular momentum l_i was taken to be equal to the critical angular momentum for fusion, l_{cr} . It is observed from Fig. 15 that, in both the cases, angular-momentum dissipation is close to the sticking limit in general, with slight discrepancy, particularly for the lighter fragments, which is discussed in the next section.

IV. RESULTS AND DISCUSSION

For both systems, it has been observed that the energy distributions were Gaussian in shape and peaked around the energies higher than those obtained from the Viola systematics. The angular distributions of the fragments showed an exponential falloff at forward angles, and the timescale of the reaction process was found to decrease with increasing fragment mass. The average Q values for both reactions decrease with the increase of emission angles and saturate at higher angles, thus signifying a fully energy damped process at these angles.

It has been observed from total-cross-section plots [Figs. 13(a) and 14(a)] that the difference in isotopic yields between the two reactions gradually decreases with the increase of neutron number for all fragments at each excitation energy. Similarly, from the relative-cross-section plots [see

Figs. 13(b) and 14(b)], it has been observed that the relative yields of the neutron-rich isotopes increase sharply in $^{20}\text{Ne} + ^{56}\text{Fe}$ ($N/Z \approx 1.11$) reaction with respect to $^{16}\text{O} + ^{58}\text{Ni}$ ($N/Z \approx 1.06$) reaction at both the excitation energies. This is the effect of the N/Z ratio of the composite since the composite in the $^{20}\text{Ne} + ^{56}\text{Fe}$ reaction is more neutron rich than the $^{16}\text{O} + ^{58}\text{Ni}$ system. Here we have observed that the mean fragment N/Z ratio of averaged over all emitted fragments (the mean average $\langle N/Z \rangle$ values are found to be ≈ 1.08 for $^{20}\text{Ne} + ^{56}\text{Fe}$ and ≈ 1.05 for $^{16}\text{O} + ^{58}\text{Ni}$ reactions at $E^* \approx 124$ MeV) depends on the N/Z ratio of the composite system [27]. It is thus evident from the above discussions that the isospin equilibrium has already taken place before the emission of the fragments from the composites for both systems at both beam energies.

Assuming a compact exit channel configuration for the fully damped part of the deep-inelastic reactions, the angular-momentum dissipation was estimated. It is apparent from Fig. 15 that, for all the reactions considered, the experimental estimates of angular-momentum dissipation for lighter fragments are slightly more than their highest limiting values predicted under the sticking condition whereas, for heavier fragments, the friction is close to the corresponding sticking limits. Microscopically, friction is generated by stochastic exchange of nucleons between the reacting partners through the window formed by the overlap of the density distributions of the two. Stronger friction, in this scenario, essentially means a larger degree of density overlap and more nucleon exchange. Consequently, lighter fragments (corresponding to more net nucleon transfer) originate from deeper collisions, for which the interaction times are larger. Therefore, the angular-momentum dissipation, originating from the stochastic nucleon exchange, may also be more, which at least qualitatively explains the observed trend. The total cross section of each fragment was also found to be more for the composite ^{74}Kr with less N/Z ratio than the composite ^{76}Kr with higher N/Z ratio at both the excitation energies. This can also be related to the microscopic phenomenon of nucleon exchange, i.e., more or less nucleon exchange required by the projectile with the target to form the corresponding emitted fragments.

V. SUMMARY AND CONCLUSIONS

Fragment emission mechanism from hot dinuclear composites formed in the reactions $^{20}\text{Ne} + ^{56}\text{Fe}$ and $^{16}\text{O} + ^{58}\text{Ni}$ has been studied at two different excitation energies. The energy and angular distributions of the emitted fragments $^{6,7}\text{Li}$, $^{7,8,9}\text{Be}$, $^{10,11}\text{Be}$, and $^{11,12,13,14}\text{C}$ have been measured in the laboratory angles ranging from 15° to 35° . From the energy and angular distributions of all the fragments, it has been observed that the fragments are emitted mostly from deep-inelastic processes for both systems. The timescales of the reactions were estimated from the fragment angular distributions and found to decrease with increasing fragment mass. The average Q values of the reactions were found to decrease with the increase of emission angles and saturate at higher angles, which signifies a fully energy damped process at higher angles. The elemental cross sections were obtained

by integrating separately the energy distributions of the fragments over the corresponding energies and over the whole angular range. It has been observed that production cross sections of all the fragments are more in $^{16}\text{O} + ^{58}\text{Ni}$ than in the $^{20}\text{Ne} + ^{56}\text{Fe}$ reaction at both excitation energies due to the easy exit channel threshold. It has been observed that the N/Z ratio of the composite plays a vital role in explaining the isotopic yield distributions of the emitted fragments, which signifies that isospin equilibrium took place prior to the breakup of the dinuclear composites at these beam energies. Assuming a compact exit channel configuration for the fully damped deep-inelastic reactions, the angular-momentum dissipation was estimated and found to be close to the corresponding phenomenological sticking limits, except for lighter

fragments. The deviation for lighter fragments may be related to the microscopic (stochastic nucleon exchange) origin of nuclear friction.

ACKNOWLEDGMENTS

The authors are thankful to the crew of cyclotron of Variable Energy Cyclotron Centre for the smooth operation of the machine during the experiments. We are also thankful to Shri Partha Dhara and his team for their support with the data-acquisition system. One of the authors (S.B.) acknowledges with thanks the financial support received as Raja Ramanna Fellow from the Department of Atomic Energy, Government of India.

-
- [1] L. G. Moretto and G. J. Wozniak, *Prog. Part. Nucl. Phys.* **21**, 401 (1988), and references therein.
- [2] R. J. Charity, M. A. McMahan, G. J. Wozniak, R. J. McDonald, L. G. Moretto, D. G. Sarantites, L. G. Sobotka, G. Guarino, A. Pantaleo, L. Fiore, A. Gobbi, and K. D. Hildenbrand, *Nucl. Phys. A* **483**, 371 (1988).
- [3] S. A. Kalandarov, G. G. Adamian, N. V. Antonenko, W. Scheid, and J. P. Wieleczko, *Phys. Rev. C* **84**, 064601 (2011).
- [4] S. J. Sanders, A. Szanto de Toledo, and C. Beck, *Phys. Rep.* **311**, 487 (1999), and references therein.
- [5] L. G. Sobotka, M. L. Padgett, G. J. Wozniak, G. Guarino, A. J. Pacheco, L. G. Moretto, Y. Chan, R. G. Stokstad, I. Tserruya, and S. Wald, *Phys. Rev. Lett.* **51**, 2187 (1983).
- [6] R. Pandey, S. Kundu, C. Bhattacharya, K. Banerjee, T. K. Rana, S. Manna, G. Mukherjee, J. K. Meena, A. Chaudhuri, T. Roy, Pratap Roy, Md. A. Asgar, V. Srivastava, A. Dey, M. Sinha, T. K. Ghosh, S. Bhattacharya, S. K. Pandit, K. Mahata, P. Patle, S. Pal, A. Shrivastava, and V. Nanal, *Phys. Rev. C* **95**, 064603 (2017).
- [7] C. Beck, B. Djerrou, B. Heusch, R. Dayras, R. M. Freeman, F. Haas, A. Hachem, J. P. Wieleczko, and M. Youlal, *Z. Phys. A: At. Nucl.* **334**, 521 (1989).
- [8] C. Beck, B. Djerrou, F. Haas, R. M. Freeman, A. Hachem, B. Heusch, A. Morsad, M. Youlal, Y. Abe, R. Dayras, J. P. Wieleczko, T. Matsuse, and S. M. Lee, *Z. Phys. A: Hadrons Nucl.* **343**, 309 (1992).
- [9] C. Beck, B. Djerrou, F. Haas, R. M. Freeman, A. Hachem, B. Heusch, A. Morsad, M. Vuillet-A-Cilles, and S. J. Sanders, *Phys. Rev. C* **47**, 2093 (1993).
- [10] B. Shivakumar, D. Shapira, P. H. Stelson, M. Beckerman, B. A. Harmon, K. Teh, and D. A. Bromley, *Phys. Rev. Lett.* **57**, 1211 (1986).
- [11] D. Shapira, J. L. C. Ford, Jr., J. Gomez del Campo, R. G. Stokstad, and R. M. DeVries, *Phys. Rev. Lett.* **43**, 1781 (1979).
- [12] C. Bhattacharya, A. Dey, S. Kundu, K. Banerjee, S. Bhattacharya, S. Mukhopadhyay *et al.*, *Phys. Rev. C* **72**, 021601(R) (2005).
- [13] D. Shapira, D. Schull, J. L. C. Ford, Jr., B. Shivakumar, R. L. Parks, R. A. Cecil, and S. T. Thornton, *Phys. Rev. Lett.* **53**, 1634 (1984).
- [14] A. Dey, C. Bhattacharya, S. Bhattacharya, T. K. Rana, S. Kundu, K. Banerjee, S. Mukhopadhyay, S. R. Banerjee, D. Gupta, and R. Saha, *Phys. Rev. C* **75**, 064606 (2007), and references therein.
- [15] A. Dey, C. Bhattacharya, S. Bhattacharya, S. Kundu, K. Banerjee, S. Mukhopadhyay, D. Gupta, T. Bhattacharjee, S. R. Banerjee, S. Bhattacharyya, T. K. Rana, S. K. Basu, R. Saha, K. Krishan, A. Mukherjee, D. Bandopadhyay, and C. Beck, *Phys. Rev. C* **76**, 034608 (2007), and references therein.
- [16] W. Dünneweber, A. Glaesner, W. Hering, D. Konnerth, R. Ritzka, W. Trombik, J. Czakanski, and W. Zipper, *Phys. Rev. Lett.* **61**, 927 (1988).
- [17] D. Shapira, R. Novotny, Y. C. Chan, K. A. Erb, J. L. C. Ford, Jr., J. C. Peng, and J. D. Moses, *Phys. Lett. B* **114**, 111 (1982).
- [18] S. Kundu, A. Dey, K. Banerjee, T. K. Rana, S. Mukhopadhyay, D. Gupta, R. Saha, S. Bhattacharya, and C. Bhattacharya, *Phys. Rev. C* **78**, 044601 (2008).
- [19] S. Kundu, C. Bhattacharya, K. Banerjee, T. K. Rana, S. Bhattacharya, A. Dey *et al.*, *Phys. Rev. C* **85**, 064607 (2012).
- [20] C. Bhattacharya, S. Bhattacharya, T. Bhattacharjee, A. Dey, S. Kundu, S. R. Banerjee, P. Das, S. K. Basu, and K. Krishan, *Phys. Rev. C* **69**, 024607 (2004), and references therein.
- [21] W. U. Schroder and J. R. Huizenga, in *Treatise on Heavy-Ion Science*, edited by D. A. Bromley, Vol. 2 of Nuclear Sciences (Plenum, New York, 1994).
- [22] N. Carlin Filho *et al.*, *Phys. Rev. C* **40**, 91 (1989).
- [23] S. J. Padalino, M. A. Putnam, J. A. Constable, T. G. De Clerck, L. C. Dennis, R. Zingarelli, R. Kline, and K. Sartor, *Phys. Rev. C* **41**, 594 (1990).
- [24] R. Eggers, M. N. Namboodiri, P. Gonthier, K. Qeoffroy, and J. B. Natowitz, *Phys. Rev. Lett.* **37**, 324 (1976), and references therein.
- [25] V. V. Volkov, in *Lecture Notes in Physics* (Springer, Berlin, 1975), Vol. 33, p. 254; *Phys. Rep.* **44**, 93 (1978).
- [26] W. U. Schroder and J. R. Huizenga, *Annu. Rev. Nucl. Sci.* **27**, 465 (1977).
- [27] A. B. McIntosh and S. J. Yennello, *Prog. Part. Nucl. Phys.* **108**, 103707 (2019).
- [28] G. A. Souliotis, P. N. Fountas, M. Veselsky, S. Galanopoulos, Z. Kohley, A. McIntosh, S. J. Yennello, and A. Bonasera, *Phys. Rev. C* **90**, 064612 (2014).
- [29] H. Y. Wu, Z. G. Xiao, G. M. Jin, B. G. Zhang, Z. Y. Li, L. M. Duan, H. W. Wang, Z. Y. Wei, Y. Y. Liu, S. F. Wang, Z. H. Lu, Y. T. Zhu, H. D. Zhu, and R. J. Hu, *Phys. Lett. B* **538**, 39 (2002).

- [30] S. Kundu, T. K. Rana, C. Bhattachary, K. Banerjee, R. Pandey, Santu Manna, J. K. Meena, A. K. Saha, J. K. Sahoo, P. Dhara, A. Dey, D. Gupta, T. K. Ghosh, Pratap Roy, G. Mukherjee, R. Mandal Saha, S. Roy, S. R. Bajirao, and S. Bhattacharya, *Nucl. Instrum. Methods Phys. Res. Sect. A* **943**, 162411 (2019).
- [31] P. Dhara, M. Dey, and A. Roy, Proc. DAE-BRNS Symp. Nucl. Phys. **46B**, 530 (2003).
- [32] P. Dhara, K. Chakraborty, M. Dey, and A. Roy, Proc. DAE-BRNS Symp. Nucl. Phys. **50**, 454 (2005).
- [33] C. Beck and A. Szanto de Toledo, *Phys. Rev. C* **53**, 1989 (1996).
- [34] V. E. Viola, K. Kwiatkowski, and M. Walker, *Phys. Rev. C* **31**, 1550 (1985).
- [35] S. Manna, T. K. Rana, C. Bhattacharya, S. Bhattacharya, S. Kundu, K. Banerjee, P. Roy, R. Pandey, V. Srivastava, A. Chaudhuri, T. Roy, T. K. Ghosh, G. Mukherjee, J. K. Meena, S. K. Pandit, K. Mahata, A. Shrivastava, and V. Nanal, *Phys. Rev. C* **94**, 051601(R) (2016).
- [36] T. K. Rana, S. Bhattacharya, C. Bhattacharya, S. Kundu, K. Banerjee, T. K. Ghosh *et al.*, *Phys. Rev. C* **88**, 021601(R) (2013).
- [37] T. K. Rana, S. Bhattacharya, C. Bhattacharya, S. Manna, S. Kundu *et al.*, *Phys. Lett. B* **793**, 130 (2019).
- [38] C. Beck *et al.*, *Eur. Phys. J. A* **2**, 281 (1998).
- [39] T. Mikumo, M. Sasagase, M. Sato, T. Ooi, Y. Higashi, Y. Nagashima, and M. Yamanouchi, *Phys. Rev. C* **21**, 620 (1980).